FED-Vol. 252, Rheology and Fluid Mechanics of Nonlinear Materials — 2000
ASME 2000

THE FLOW OF UCM AND OLDROYD-B FLUIDS PAST A CYLINDER

Manuel A. Alves
Departamento de Engenharia Química, CEFT
Faculdade de Engenharia
Universidade do Porto, Rua dos Bragas
4050-123 Porto, Portugal, mmalves@fe.up.pt

Fernando T. Pinho
Centro de Estudos de Fenómenos de Transporte
DEMEGI, Faculdade de Engenharia
Universidade do Porto, Rua dos Bragas
4050-123 Porto, Portugal,fpinho@fe.up.pt

Paulo J. Oliveira
Departamento de Engenharia Electromecânica
Universidade da Beira Interior
Rua Marquês D'Ávila e Bolama, 6200 Covilhã, Portugal
pjpo@ubi.pt

ABSTRACT

Accurate solutions are obtained with the numerical method of Oliveira et al (1998) for the inertialess plane flow around a confined cylinder. This numerical procedure is based on the finite-volume method in non-orthogonal block-structured meshes with a collocated arrangement of the dependent variables, and makes use of a special interpolation practice to avoid stress-velocity decoupling. Two high-resolution schemes are implemented to represent the convective terms in the constitutive equations for the upper convected Maxwell and Oldroyd-B fluids, and the resulting predictions of the drag coefficient on the cylinder are shown to be as accurate as existing finite-element method predictions based on the very accurate h-p refinement technique.

KEYWORDS: Cylinder; Viscoelastic; High-Resolution.

1. INTRODUCTION

The increasing use of computational tools to design industrial equipment requires the ability of existing methods to predict accurately the flow of viscoelastic fluids and in this respect one of the relevant benchmark test cases is the two-dimensional flow around a cylinder (Brown and McKinley, 1994). This flow is classified as a "smooth flow" because it does not possess any geometrical singularity, but still there are difficulties associated with the development of thin stress layers and high stress values on the cylinder surface and along the centreline in the cylinder wake, which restrict the range of Deborah numbers (*De*) for which steady solutions are obtained.

The general collocated FVM procedure for viscoelastic flows developed by Oliveira et al (1998) uses non-orthogonal, collocated, semi-structured grids to allow the mapping of complex geometries. More recently, Oliveira and Pinho (1999a) performed simulations with formally second-order interpolation schemes for the discretisation of the convective terms in the constitutive equation and assessed the advantages and shortcomings when this scheme was the second-order upwind. In this latter study it became apparent that in order to improve the stability of the method and accuracy of the predictions one had to resort to bounded high-resolution interpolation schemes for convection. That has been accomplished by Alves et al (2000) who demonstrated the method with the difficult 4:1 plane contraction flow. In the present paper, a second, more accurate high-resolution interpolation scheme is implemented for enhanced accuracy and the formulation is tested with the benchmark problem of the flow past a confined cylinder (blockage ratio 0.5), with both upper convected Maxwell (UCM) and Oldroyd-B fluids. This smooth problem requires nonorthogonal meshes and allows comparison of the drag force on the cylinder (the benchmark result) with values from other simulations in the literature [Liu et al (1998), Dou and Phan-Thien (1999), Fan et al (1999), Sun et al (1999)] thus enabling a direct assessment of the accuracy of the present FVM.

2. GOVERNING EQUATIONS

The method solves the system of equations for incompressible flow, made up of conservation of mass and of linear momentum:

$$\frac{\partial u_i}{\partial x_i} = 0 \tag{1}$$

$$\frac{\partial \rho u_i}{\partial t} + \frac{\partial \rho u_j u_i}{\partial x_j} = -\frac{\partial p}{\partial x_i} + \frac{\partial \tau_{ij_{tot}}}{\partial x_j} \tag{2}$$

and the rheological constitutive model for an Oldroyd-B fluid which is written as the sum of a Newtonian solvent (Eq. 3-a) with an upper convective Maxwell model (Eq. 3-b)

$$\tau_{ij_{tot}} = \eta_s \left(\frac{\partial u_i}{\partial x_j} + \frac{\partial u_j}{\partial x_i} \right) + \tau_{ij} \tag{3-a}$$

$$\tau_{ij} + \lambda \left(\frac{\partial \tau_{ij}}{\partial t} + u_k \frac{\partial \tau_{ij}}{\partial x_k} \right) = \eta_p \left(\frac{\partial u_i}{\partial x_j} + \frac{\partial u_j}{\partial x_i} \right) + \lambda \left(\tau_{jk} \frac{\partial u_i}{\partial x_k} + \tau_{ik} \frac{\partial u_j}{\partial x_k} \right) \tag{3-b}$$

In the above equations Einstein's summation convention applies, ρ is the density of the fluid, u_i is the velocity component along the Cartesian co-ordinate x_i, p is the pressure, λ is the relaxation time, η_s is the shear viscosity of the Newtonian solvent and η_p is the contribution of the polymer to the total shear-viscosity. The dependent variables solved for in Eqs (3) are the polymer stress components τ_{ij} and there is no need to store the total stress $\tau_{ij\,tot}$.

Although we are here concerned with steady flows, the numerical method approaches that steady state by a time marching sequence, so the inertia term in Eqs. (2) and (3-b) are retained. This time-marching approach offers the advantage of being able to capture possible unsteady phenomena. It is also noted that we adopt the notation of writing on the left-hand-side of Eqs. (2) and (3-b) the terms which will be dealt with implicitly in the numerical procedure, and on the right-hand-side those dealt with explicitly (these go into the source term of the matrix equations).

3. NUMERICAL METHOD

The equations of the previous section are transformed into a general nonorthogonal co-ordinate system for easy application of the FVM method to a collocated mesh arrangement. The equations are then integrated over the set of control volumes (cells) and discretised. The dependent variables remain the Cartesian velocity and polymer stress components and the pressure, all stored at the centre of the cells. To avoid stress-velocity decoupling, the special procedure developed previously [Oliveira et al (1998), Oliveira and Pinho (1999b)] for the calculation of the divergence of the stress term in the momentum equation is adopted. The novelty here is the implementation of the high-resolution schemes used to discretise the convective terms in the constitutive equation and only this will be addressed in detail below.

3.1 Constitutive equation

After discretisation, the constitutive equation (3-b) for a general cell P of volume V_P is written under a linearised form as

$$a_P \tau_{ij,P} - \sum_F a_F \tau_{ij,F} = S_{\tau_{ij}} + \frac{\lambda V_P}{\delta t} \tau^0_{ij,P} \qquad (4)$$

where $\tau_{ij,P}$ is the stress in the cell, $\tau_{ij,F}$ are stresses in neighbouring cells and δt is the time step. As there is no diffusion term in the original constitutive equation, the coefficients a_F are composed by convective contributions only. When these are based on the upwind differencing scheme (UDS), the following results

$$a_F = -\frac{\lambda}{\rho} \min(F_f, 0) \qquad (5)$$

where F_f represents the mass flow rate across the face f between cells P and F, which is evaluated as described in Issa and Oliveira (1994). However, the convective terms are not discretised with UDS but with the high-resolution schemes (HRS) to be described in the next section. This will not change the coefficients of the stress equation, which are still based on Eq. (5), and the effect of the HRS will be introduced through the deferred correction approach (Khosla and Rubin, 1974) as explained by Alves et al (2000). This is a very convenient approach because it allows for a unified implementation of various HRS.

The remaining terms in the discretised Eq. (4) are the central coefficient, given by

$$a_P = V_P + \sum_F a_F + \frac{\lambda V_P}{\delta t} \qquad (6)$$

and the source term, which will incorporate the following three contributions:

(i) part of the Oldroyd derivative on the r.h.s of Eq. (3-b), which is evaluated with the central differencing scheme (CDS);

(ii) the viscous part of the stresses, also evaluated with CDS;

(iii) and the additional term due to implementation of the HRS by deferred correction, which is given by the difference between the convected stress fluxes based on HRS and those based on UDS.

3.2 High-resolution differencing schemes

These are based on the normalized variable and space formulation (NVSF) of Darwish and Moukalled (1996) whereby the convected stress component τ_{ij} and the general curvilinear co-ordinate ξ are normalised as

$$\tilde{\tau}_{ij} = \frac{\tau_{ij} - \tau_{ij,U}}{\tau_{ij,D} - \tau_{ij,U}} \qquad (7)$$

$$\tilde{\xi} = \frac{\xi - \xi_U}{\xi_D - \xi_U} \qquad (8)$$

where the subscripts U and D refer to the upstream and downstream cells to cell P which is the cell immediately upstream of cell face f under consideration. To satisfy the convection boundedness criterion (CBC) of Gaskell and Lau (1988) the functional $\tilde{\tau}_{ij,f} = fn(\tilde{\tau}_{ij,P})$ must be represented by the shadowed region in the normalised variable diagram of Fig. 1 and the straight line of slope 1 outside the triangle.

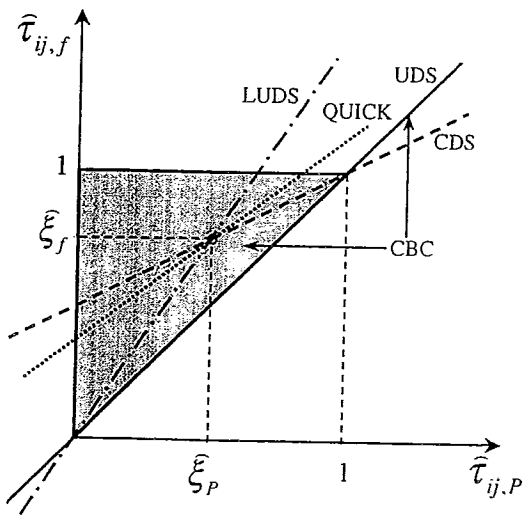

Figure 1- Representation of the differencing schemes in the normalised variable and space formulation.

Two high-resolution schemes are implemented in this work: the MINMOD of Harten (1983) and the SMART of Gaskell and Lau (1988). In isolation, the high-order differencing schemes fail to satisfy the convection boundedness criterion, but if appropriately combined

as in these two high-resolution schemes, they become bounded. Using the NVSF formulation, the face stresses can be expressed as

$$\tilde{\tau}_{ij.f} = a + b\tilde{\tau}_{ij.P} \tag{9}$$

where MINMOD and SMART are expressed analytically by Eqs. (10) and (11), respectively:

$$\tilde{\tau}_{ij.f} = \begin{cases} \dfrac{\tilde{\xi}_f}{\tilde{\xi}_P}\tilde{\tau}_{ij.P} & 0 < \tilde{\tau}_{ij.P} < \tilde{\xi}_P \quad \text{(LUDS)} \\ \dfrac{1-\tilde{\xi}_f}{1-\tilde{\xi}_P}\tilde{\tau}_{ij.P} + \dfrac{\tilde{\xi}_f - \tilde{\xi}_P}{1-\tilde{\xi}_P} & \tilde{\xi}_P \le \tilde{\tau}_{ij.P} < 1 \quad \text{(CDS)} \\ \tilde{\tau}_{ij.P} & \text{elsewhere} \quad \text{(UDS)} \end{cases} \tag{10}$$

$$\tilde{\tau}_{ij.f} = \begin{cases} \dfrac{\tilde{\xi}_f\left(1-3\tilde{\xi}_P+2\tilde{\xi}_f\right)}{\tilde{\xi}_P\left(1-\tilde{\xi}_P\right)}\tilde{\tau}_{ij.P} & 0 < \tilde{\tau}_{ij.P} < \dfrac{\tilde{\xi}_P}{3} \\ \dfrac{\tilde{\xi}_f\left(1-\tilde{\xi}_f\right)}{\tilde{\xi}_P\left(1-\tilde{\xi}_P\right)}\tilde{\tau}_{ij.P} + \dfrac{\tilde{\xi}_f\left(\tilde{\xi}_f-\tilde{\xi}_P\right)}{1-\tilde{\xi}_P} & \dfrac{\tilde{\xi}_P}{3} \le \tilde{\tau}_{ij.P} < \dfrac{\tilde{\xi}_P}{\tilde{\xi}_f}\left(1+\tilde{\xi}_f-\tilde{\xi}_P\right) \\ \quad \text{(QUICK)} & \\ 1 & \dfrac{\tilde{\xi}_P}{\tilde{\xi}_f}\left(1+\tilde{\xi}_f-\tilde{\xi}_P\right) \le \tilde{\tau}_{ij.P} < 1 \\ \tilde{\tau}_{ij.P} & \text{elsewhere} \quad \text{(UDS)} \end{cases} \tag{11}$$

Stress fluxes are evaluated based on Eq. (10) or (11) for each of the six faces of a cell, are summed (with incoming fluxes taken as negative), and are then incorporated into the source term of the stress equation $S_{\tau_{ij}}$ following the deferred correction approach.

3.3 Solution procedure

The discretised sets of equations for each variable are solved sequentially in a decoupled manner and the revised version of the SIMPLEC algorithm (Van Doormal and Raithby, 1984), as explained in Oliveira et al (1998), is used to ensure conservation of mass and momentum by the pressure and velocity fields. The original algorithm is only marginally affected by extension to viscoelastic flow calculations, is not affected by the adoption of the HR scheme and is independent of the constitutive equation chosen. Implicit solution of the linear sets of equations was carried out iteratively with standard pre-conditioned symmetric or bi-conjugate gradient methods (Meijerink and Van der Vorst, 1977).

4. NUMERICAL RESULTS AND DISCUSSION

4.1 Flow Conditions

We consider the plane flow past a circular cylinder of radius R placed perpendicularly at the centreline of a channel of height $2h$ defining a blockage ratio of 50% (h/R=2). The computational domain is $80R$ long, with $19R$ upstream and $59R$ downstream of the forward and rear stagnation points of the cylinder, respectively. No-slip conditions are imposed at both the cylinder surface (r=R) and the channel wall (y=h) where the stress components are obtained from solution of the constitutive equations. Due to symmetry of the geometry only the upper half of the domain was used in the calculations, with symmetry boundary conditions imposed on the centreplane.

All the calculations were carried out for the limiting case of Re=0, and the remaining relevant nondimensional quantity is the Deborah number defined in the usual way as

$$De = \frac{\lambda U}{R} \tag{12}$$

where U represents the bulk velocity in the channel. The ratio of solvent to total viscosity of the Oldroyd-B fluid was set to be the same as in other works in the literature, as

$$\frac{\eta_s}{\eta_s + \eta_p} = 0.59 \tag{13}$$

Several consistently refined meshes have been used in order to quantify the discretization errors. These meshes are denoted as M60, M120, etc, where the figure after the M denotes the number of radial cells from the cylinder surface to the channel wall.

4.2 Order of convergence

The dimensionless drag coefficient C_d is calculated from surface integration of the stress and pressure fields around the cylinder:

$$C_d \equiv \frac{1}{\eta U}\int_S (\tau_{tot} - p\mathbf{I})\mathbf{n}.\hat{\mathbf{i}}\, dS \tag{14}$$

where $\mathbf{I}$ is the identity tensor, $\mathbf{n}$ the unit normal vector to the cylinder surface and $\hat{\mathbf{i}}$ is the unit vector in the x-direction.

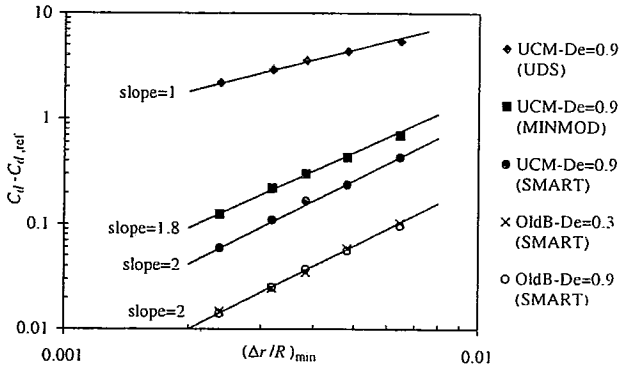

Figure 2- Estimated error versus minimum cell size.

A simple trial and error method to evaluate the order of convergence of the method assumes that the extrapolated C_d from Richardson's technique represents the exact (reference) solution and plots the variation of the estimated error $|C_d - C_{d,ref}|$ as a function of $(\Delta r/R)_{min}$ in log-log coordinates, the slope of which then gives the order of convergence, as shown in Fig. 2. As an estimate of the exact C_d, taken as the reference value, $C_{d,ref}$, the extrapolated value from the SMART calculations was used in all cases, as that was the most accurate scheme in this study. Fig. 2 also demonstrates that the asymptotic range of C_d is achieved in the four finer meshes, for the relatively high De=0.9 and for both the UCM and Oldroyd-B fluids. The orders of convergence of the various methods were thus determined and are listed in Table 1: second-order for MINMOD and SMART, with SMART slightly more accurate than MINMOD, and first-order for UDS.

Table 1- Order of convergence of the numerical simulations

	UCM			OLD-B
De	UDS	MINMOD	SMART	SMART
0.3	1.1	1.9	2.0	2.0
0.9	0.9	1.8	2.0	2.0

4.3 Upper convected Maxwell fluids

Figure 3(*a*) compares our extrapolated values of C_d with those of Fan et al (1999), obtained with FEM and their MIX1 formulation, and with the CVFEM results of Phan-Thien and Dou (1999). The present results obtained with SMART scheme in mesh M120 and the extrapolated curves based on results with the SMART and MINMOD high-resolution schemes basically collapse. There is excellent agreement between our results and Fan et al (1999) predictions, who used a very accurate FEM h-p refinement technique (with polynomials of up to 6th order), and both sets are well below the predictions of Phan-Thien and Dou (1999).

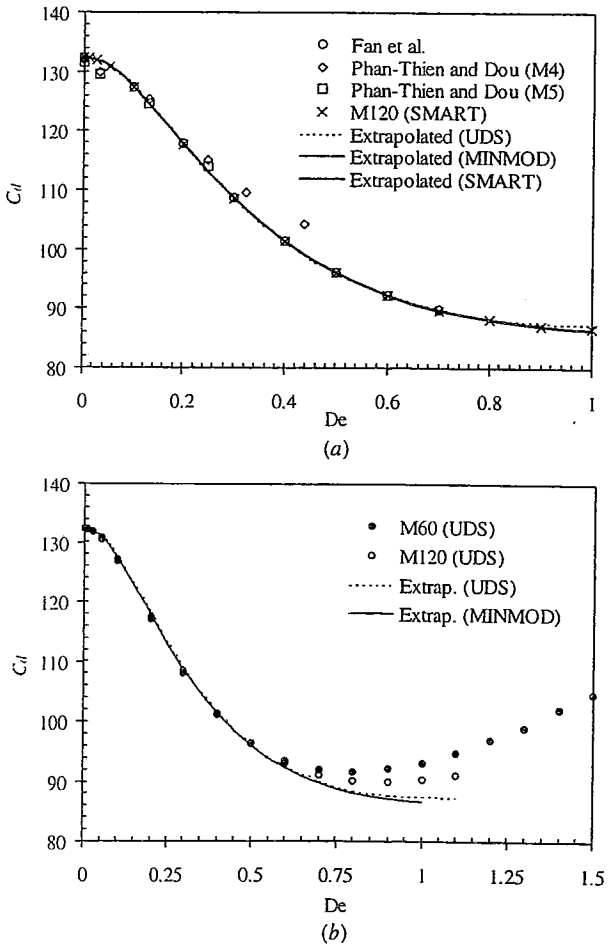

Figure 3- Drag coefficient as a function of the Deborah number for UCM fluids. (a) Comparison with data from the literature; (b) predictions with the upwind scheme (UDS).

What is evident from Fig. 3(*b*) is that as *De* increases, the inaccuracies in the predicted C_d with the lower order scheme tend to progressively increase, the C_d value itself tends to be higher than the "exact" solution and, furthermore, it starts increasing whereas the best predictions show an asymptotic minimum level of C_d for high *De*.

Normal stress profiles around the cylinder and along the centreline show two maxima as illustrated in Fig. 4 for *De*=0.6. The first maximum is within the thin boundary layer over the cylinder surface and the second maximum is in the wake, some distance downstream from the rear stagnation point. The present numerical method shows somewhat more robustness compared with Fan et al (1998), in spite of being a decoupled procedure: we were able to obtain converged solutions with the high resolution schemes MINMOD and SMART up to *De*= 1 and 0.9, respectively, whereas the MIX1 calculations of Fan et al (1999) diverged for *De*> 0.75.

At the moderate value of De=0.6 the contribution of the polymer to the longitudinal normal stress predictions in Fig. 4 are very close to those of Fan et al (1999), except in the stress wake where the predictions with the fine mesh M120 fall somewhat lower. However, by refining the mesh in that area, especially in the direction tangential to the cylinder surface (that is, the θ-direction for a cylindrical coordinate system centred in the cylinder axis), we are then able to match closely Fan et al's predictions in the wake. Figure 4 also demonstrates the improved convergence and accuracy brought about by the high-resolution schemes. The MINMOD predictions are far less affected by mesh fineness and are in better agreement with the high-order h-p FEM results of Fan et al (1999). Agreement in the stress boundary layer around the cylinder is reflected in the coincidence of C_d values exhibited in Fig. 3(*a*).

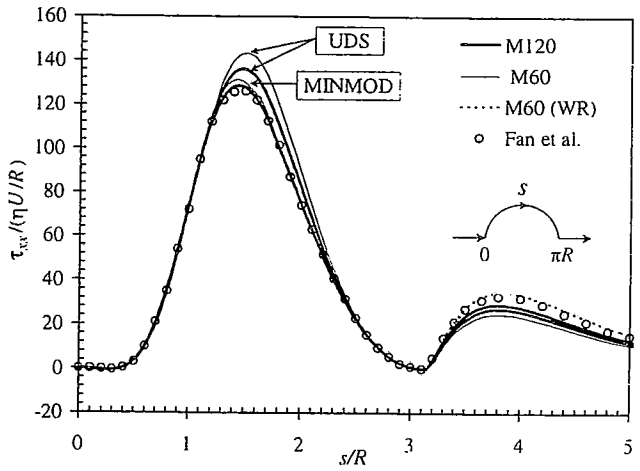

Figure 4- Influence of interpolation scheme and mesh refinement on the predicted τ_{xx} along cylinder wall and wake centerline. Comparison with Fan el al (1999) predictions at *De*=0.6.

At *De*>1 we can no longer obtain converged solutions. A possible cause for the numerical problems leading to convergence breakdown could be related to the pressure variation around the cylinder wall and centreline, which is shown for various *De* values in Fig. 5. As *De* increases the pressure on the cylinder forward and rear surfaces

increase progressively, but smoothly, due to the shifted flow pattern and results in the reduced drag. Within the rear stagnation point region a different situation arises: at low Deborah numbers the pressure level tends to rise steadily with De. At a critical Deborah number between 0.3 and 0.6 the behaviour of the rear stagnation point pressure reverses: a point of highly-negative peak pressure develops and becomes more pronounced as De increases. At $De \approx 0.9$ that point has developed into a wake singularity.

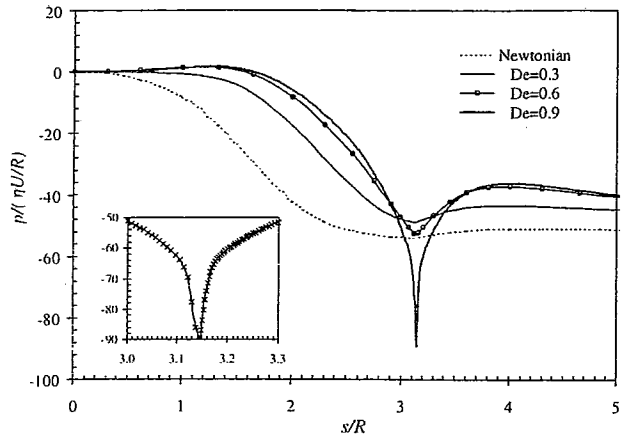

Figure 5- Influence of Deborah number on the pressure distribution around the cylinder surface and along the wake centreline (SMART scheme; p=0 at forward stagnation point).

4.4 Oldroyd-B fluids

For the Oldroyd-B fluid the calculations have been carried out with the SMART scheme only since it is the most accurate, and the drag coefficient predictions are compared with the FEM results of: Fan et al (1999) with the MIX1 formulation; Sun et al (1999) with the DAVSS-G/DG formulation; Liu et al (1998) with the DEVSS-G/SUPG formulation; and Dou and Phan-Thien (1999) with the CVFEM method and the DAVSS-ω formulation.

The C_d results are plotted in Fig. 6 and again there is excellent agreement between the finer mesh predictions, our Richardson's extrapolated results (not far from the M120 results), and the FEM predictions of Fan et al (1999) (differences below 0.1%, often below 0.01%). The loss of accuracy of the CVFEM method of Dou and Phan-Thien (1999) is evident for $De \geq 0.3$, and the FEM predictions of the MIT group, Liu et al (1998) and Sun et al (1999), are just somewhat higher for $De \geq 0.5$. Sun et al (1999), who used a FEM with quadratic continuous polynomials for the velocity and linear for the pressure fields, have shown their method to be second-order accurate in a lower blockage cylinder flow (h/R=8) at low Deborah numbers ($De \leq 1.0$). For the present 50% blockage ratio their smallest mesh size is only $(\Delta s/R)_{\min} = 0.056$ and improvements in their predictions would require further refinement especially at high Deborah numbers.

In contrast to the UCM predictions, the Oldroyd-B fluid exhibits an increase of C_d at high Deborah numbers, with a minimum drag coefficient occurring at $De \cong 0.75$. At De= 1 all methods still give converged solutions and the literature shows that the calculations are more stable with Oldroyd-B fluids than with UCM fluids.

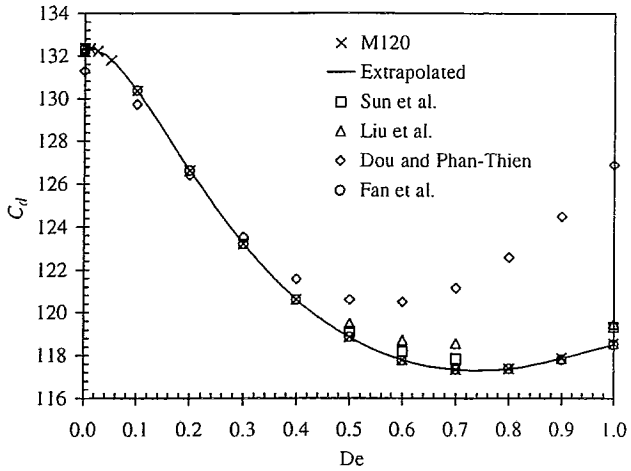

Figure 6- Drag coefficient as a function of Deborah number for Oldroyd-B fluids.

A detailed comparison of the longitudinal normal stress variation along the centreline and cylinder surface is seen in Fig. 7, at the moderate to high Deborah number of 0.7. The fine mesh (M120) predictions closely match Fan et al's and the difference between M60 and M120 predictions are only apparent near the wake maximum, where the wake-refined mesh is again required to resolve the stress growth and thus to provide good agreement with Fan et al (1999) results. For higher Deborah numbers our C_d still follows Fan et al's closely but the discrepancies in the wake region near the point of maximum τ_{xx} are accentuated. These discrepancies are confined to the near wake region and do not seem to affect the stress field upstream, around the cylinder.

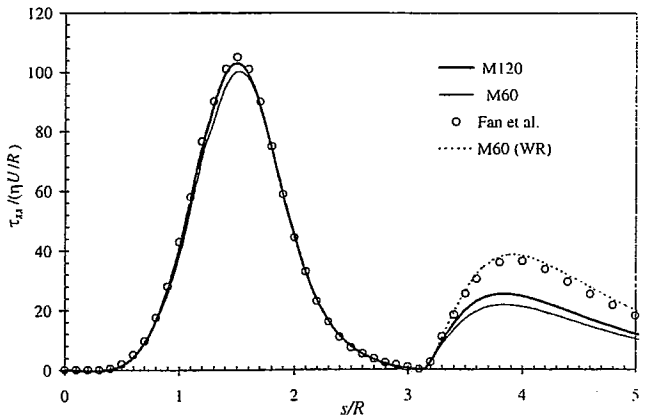

Figure 7- Influence of mesh refinement on τ_{xx} along cylinder wall and wake centreline, and comparison with literature for Oldroyd-B fluids (SMART scheme; De=0.7).

In Fig. 8 some contour plots are displayed for the Newtonian case and for the Oldroyd-B fluid at De=0.9. The differences are notorious, especially for v and for the stresses in the downstream part of the channel.

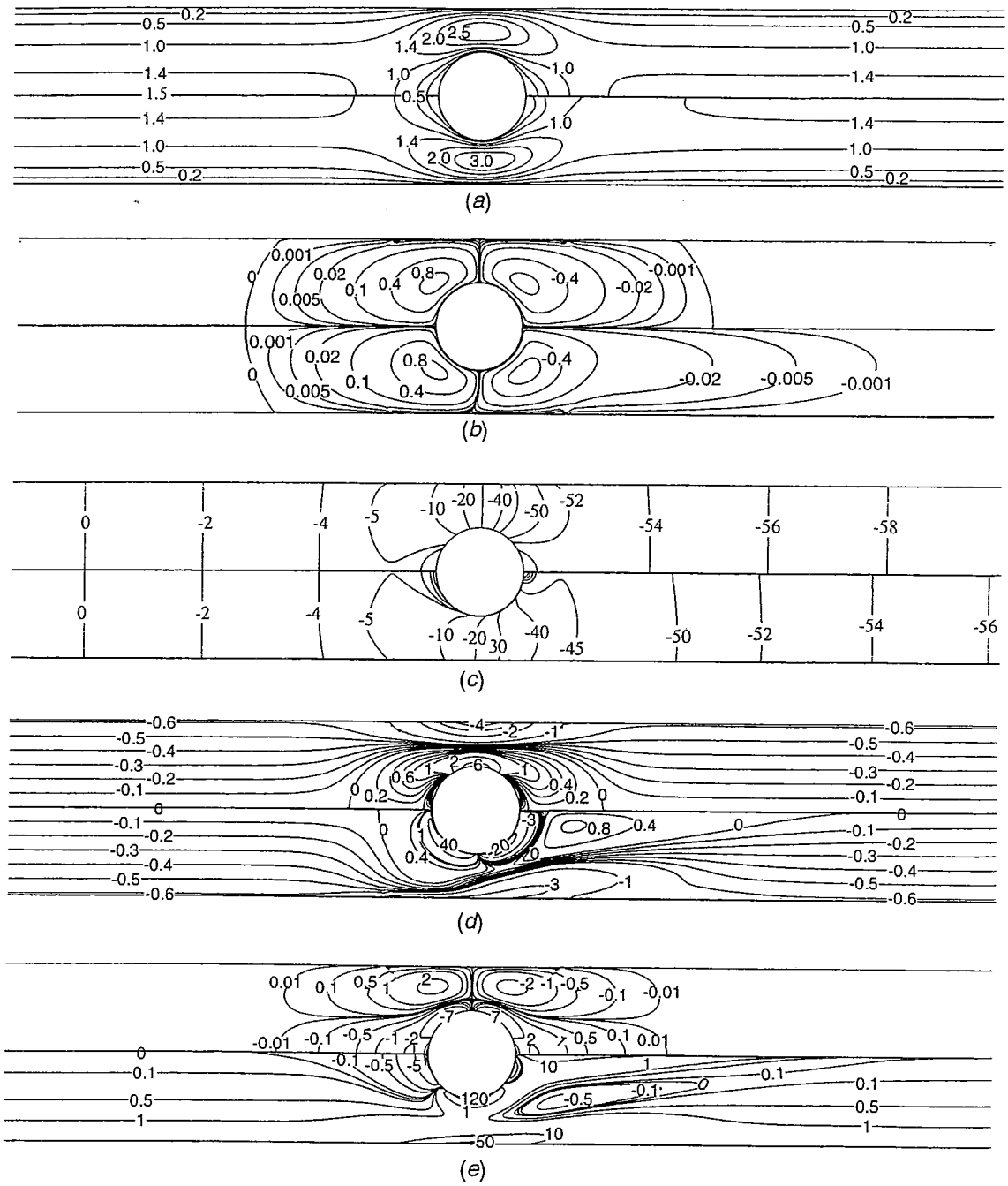

Figure 8- Contour plots of dimensionless variables: (*a*) u/U; (*b*) v/U; (*c*) $p/(\eta U/R)$; (*d*) $\tau_{xy}/(\eta U/R)$; (*e*)$N_1/(\eta U/R)$. Upper half corresponds to the Newtonian case, and lower half to the Oldroyd-B fluid at *De*=0.9. Flow is from left to right.

A detailed difference with the UCM is the velocity distribution along the centreline of the channel near the rear stagnation point. The downstream shift of the streamlines is still present far from the back of the cylinder, resulting in the observed decrease of C_d at low and moderate Deborah numbers, but the upstream shift at higher Deborah numbers occurs over a much wider zone close to the rear stagnation point, as shown in Fig. 9. Similar behaviour has been reported for the corresponding falling-sphere-in-a-tube problem (Bush, 1993) and in our previous study for the flow past a cylinder (Oliveira et al, 1998).

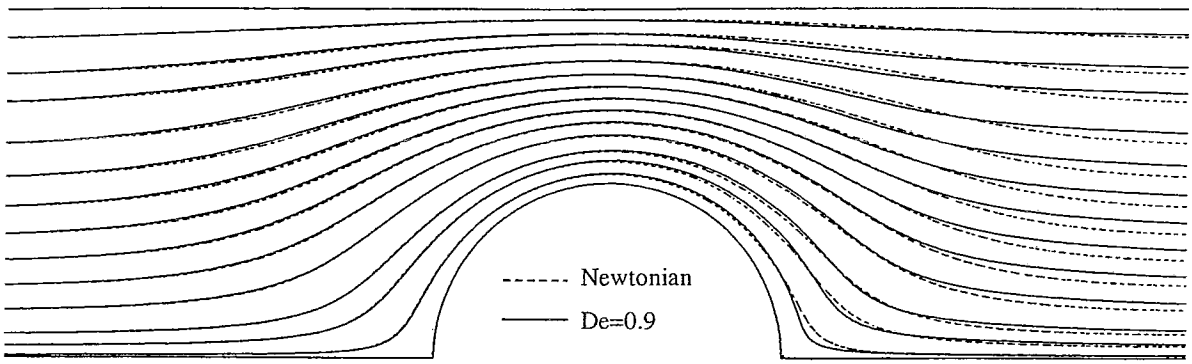

Figure 9- Zoomed view of the streamlines for a Newtonian fluid (dashed lines) and an Oldroyd-B fluid at *De*=0.9 (full lines).

CONCLUSIONS

Accurate predictions for the flow around a confined cylinder (blockage ratio 0.5) are obtained with a general collocated FVM incorporating two high-resolution schemes to represent the convective terms in the constitutive equation: MINMOD and SMART. A consistent mesh refinement study and the application of Richardson's extrapolation to the solution functional C_d allowed us to determine the observed order of convergence of the schemes: 2.0 for SMART; 1.8 for MINMOD; and 0.9 for upwind differencing.

For this problem, which is usually classified under the category of "smooth flow", we have consistent predictions of C_d up to $De \approx 0.7$ between the present FVM and the FEM of Fan et al (1999) who used an highly accurate h-p refinement technique with polynomials of degree up to 6. Other FEM and CVFEM results from the literature start overpredicting the present C_d data and that of Fan et al (1999) at $De \approx 0.3$ (UCM) and $De \approx 0.4$ (Oldroyd-B), an indication of loss of accuracy. It is thus established that FVM can yield accurate results, provided the discretisation of the constitutive equation and the level of mesh refinement are adequate.

ACKNOWLEDGEMENTS

M. A. Alves is a member of staff at Departamento de Engenharia Química, FEUP, and wishes to thank his colleagues for a temporary leave of absence. P. J. Oliveira thanks Unidade de Materiais Têxteis e Papeleiros of UBI.

REFERENCES

Alves, M. A., Pinho, F. T., and Oliveira, P. J., 2000, J. Non-Newt. Fluid Mech., Vol. 93, pp. 287-314.

Brown, R. A., and McKinley, G. H., 1994, J. Non-Newt. Fluid Mech., Vol. 52, pp. 407-413.

Bush, M. B., 1993, J. Non-Newt. Fluid Mech., Vol. 49, pp. 103-122.

Darwish, M. S., and Moukalled, F., 1996, Num. Heat Transfer, Part B, Vol. 30, pp. 217-237.

Dou, H.- S., and Phan-Thien, N., 1999, J. Non-Newt. Fluid Mech., Vol. 87, pp. 47-73.

Fan, Y., Tanner, R. I., and Phan-Thien, N., 1999, J. Non-Newt. Fluid Mech., Vol. 84, pp. 233-256.

Gaskell, P. H., and Lau, A. K. C., 1988, Int. J. Numer. Meth. Fluids, Vol. 8, pp. 617-641.

Harten, A., 1983, J. Comput. Physics, Vol. 49, pp. 357-393.

Issa, R. I., and Oliveira, P. J., 1994, Computers and Fluids, Vol. 23, pp. 347-372.

Khosla, P. K., and Rubin, S. G., 1974, Comput. and Fluids, Vol. 2, pp. 207-209.

Liu, A. W., Bornside, D. E., Armstrong, R. C., and Brown, R. A., 1998, J. Non- Newt. Fluid Mech., Vol. 77, pp. 153-190.

Meijerink, J. A., and Van Der Vorst, H. A., 1977, Math. Comput., Vol. 31, pp. 148.

Oliveira, P. J., Pinho, F. T., and Pinto, G. A., 1998, J. Non-Newt. Fluid Mech., Vol. 79, pp. 1-43.

Oliveira, P. J., and Pinho, F. T., 1999a, J. Non-Newt. Fluid Mech., Vol. 88, pp. 63-88.

Oliveira, P. J., and Pinho, F. T., 1999b, Numerical Heat Transfer, Part B, Vol. 35, pp. 295-315.

Phan-Thien, N., and Dou, H.- S., 1999, Comput. Methods Appl. Mech. Engrg., Vol. 180, pp. 243-266.

Sun, J., Smith, M. D., Armstrong, R. C., and Brown, R. A., 1999, J. Non-Newt Fluid Mech., Vol. 86, pp. 281-307.

Van Doormal, J. P., and Raithby, G. D., 1984, Num Heat Transfer, Vol. 7, pp. 147-163.